Int J Thermophys (2009) 30:1536–1556
DOI 10.1007/s10765-009-0645-8

Theoretical Analysis of Pulsed Photoacoustic Effect in Solids

Alina Domanowska · Roman J. Bukowski

Received: 31 December 2008 / Accepted: 17 August 2009 / Published online: 2 September 2009

Abstract This article presents a one-dimensional theory of a photoacoustic cell, working in the pulse regime. A four-layer system with elements of finite thickness has been assumed to represent consecutive parts of the photoacoustic cell. A parabolic heat equation with an instantaneous, bulk heat source has been solved using the Fourier transform of spatial coordinates. The theory allows one to assume that a heat source is existing in every part of the system and that an arbitrary time profile of the initial pulse is applied. Consequently, the system can be treated as an arbitrary photothermic or photoacoustic one-dimensional system. As a result, one obtains temperature profiles in the entire system at any time instant after its excitation with a light pulse. The gas-pressure evolution is dependent on the thermal and optical properties of the sample, the cell geometry, and duration and shape of the initial pulse.

Keywords Heat-pulse propagation in solids · Photoacoustic effect · Piezo-, elasto-, and acousto-optical effects · Thermo-optical and photothermal effects

1 Introduction

Methods to measure thermal and optical parameters of solid materials based on the photoacoustic effect have been successfully developed for many years. Traditional ones use modulated light sources and are applied to determine thermal and optical parameters of solids, especially in cases when other methods of measurement fail. They allow, for example, determination of the absorption coefficient of weakly or strongly absorbing materials, and thermal parameters of thin films or very small

A. Domanowska (✉) · R. J. Bukowski
Institute of Physics, Silesian University of Technology, Ul. Krzywoustego 2, 44-100 Gliwice, Poland
e-mail: Alina.Domanowska@polsl.pl

samples. Photoacoustic investigations are non-destructive, which allows for repetitive measurements of different parameters using the same sample.

The basic advantage of photoacoustic spectroscopy is that the resulting signal consists only of the absorbed portion of the incident energy. Since the amplitude of the signal is proportional to the amount of heat transferred from the sample to the gas (up to the saturation level), a strict dependence exists between the magnitude of the photoacoustic signal and the amount of energy absorbed by the sample [1].

In conventional photoacoustic methods, the exciting signal of a given wavelength is periodically modulated while the amplitude and the phase of the acoustic response's variable component are the subjects of the measurement. A special case of the photoacoustic method is the pulsed photoacoustic method, where the exciting signal is either a single light pulse or a series of pulses separated with time gaps, allowing the system to return to the unexcited state before the next pulse. The response of an experimental system to pulse excitation contains information on optical (light absorption) and thermal (conductivity, capacity, and diffusivity) properties of the material under investigation. The experiment may be carried out using the photoacoustic device for continuous wave measurements, but the received photoacoustic signal is more difficult to interpret due to its wide frequency bandwidth. To understand and correctly interpret a pulsed signal, it is necessary to carry out a theoretical analysis, taking into account such a specific way of the exciting signal modulation.

Existing theoretical models of this effect might be insufficient for the analysis of experimental signals, since they take into account only the layer of the sample isolated thermally from its surroundings as in Parker et al. [2] or utilize an electrically initiated pulsed heat source as in [3], or assume infinite dimensions of the backing and the window, light absorption only in the sample, and the simplest rectangular exciting pulse [4,5]. A model, allowing consideration of as many properties of a pulse-excited photoacoustic cell as possible, is needed. Such a model is presented in this article, and the above-cited theories have been used to verify its correctness.

2 Theoretical Model

A photoacoustic cell is a basic unit of testing equipment used in photoacoustic investigations. The basic elements that must be taken into account in a mathematical model of the cell are backing, sample, gas, and window. In this article, the following system geometry has been assumed (Fig. 1): backing in the area $-\mathrm{b} \leq x \leq 0$, sample $0 \leq x \leq \mathrm{l}$, gas $\mathrm{l} \leq x \leq \mathrm{g}$, and window $\mathrm{g} \leq x \leq \mathrm{w}$, but in summary, the sequence and number of layers could be optional. The heat source may exist in each element of the system; it is therefore necessary to solve the heat equation with a heat source for each area of the cell.

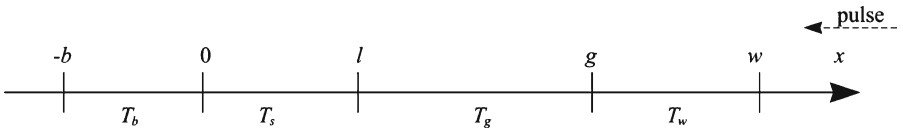

Fig. 1 One-dimensional model of the photoacoustic cell

2.1 Boundary Problem

To calculate temperature fields in individual segments of a one-dimensional photoacoustic cell as shown in Fig. 1 after its excitation with a light pulse, one has to solve the parabolic heat equation for each defined area:

$$\frac{\partial^2 T_i}{\partial x^2} - \frac{1}{\alpha_i}\frac{\partial T_i}{\partial t} = -\frac{g_i(x,t)}{\kappa_i}, \tag{1}$$

where i = b, s, g, or w for backing, sample, gas, and window, respectively. α_i is the thermal diffusivity and κ_i is the thermal conductivity of the ith cell element.

The received general solutions for each area are later joined with a set of boundary conditions of the second type on interfaces for heat fluxes on the left and right boundaries of the area;

$$\begin{aligned} -\kappa_i \frac{\partial T_i}{\partial x}\bigg|_{\substack{\text{left}\\ \text{boundary}}} &= q_{\text{left}}(t), \\ -\kappa_i \frac{\partial T_i}{\partial x}\bigg|_{\substack{\text{right}\\ \text{boundary}}} &= q_{\text{right}}(t), \end{aligned} \tag{2}$$

and with initial condition,

$$T_i(x,0) = T_0. \tag{3}$$

For such assumed boundary conditions, the solution may be obtained with different methods [6–8], and the result will not depend on the chosen method. One of them is to use the Fourier transform for the spatial coordinate;

$$\hat{T}(\xi,t) = \int_0^{l_i} T(x,t)\cos(\xi x)\,\mathrm{d}x, \tag{4}$$

where l_i is the thickness of the ith element.

This method with a more general case of boundary conditions has been presented in [8]. The solution for boundary conditions (Eq. 2) has, however, a slightly different form,

$$\begin{aligned} T_i(x,t) = T_0 + \frac{\alpha_i}{\kappa_i l_i}\int_{-\infty}^{t} \left[q_{\text{left}}(t')(1+2S_1) - (-1)^n q_{\text{right}}(t')(1+2S_2)\right]\mathrm{d}t' \\ + \frac{\alpha_i}{\kappa_i l_i} G_i(x,t), \end{aligned} \tag{5}$$

where l_i is the thickness of the i-numbered cell element and

$$S_1 = \sum_{n=1}^{\infty} \exp\left[-\alpha_i \xi_n^2 (t - t')\right] \cos(\xi_n x), \quad \xi_n = \frac{n\pi}{l_i},$$
$$S_2 = \sum_{n=1}^{\infty} (-1)^n \exp\left[-\alpha_i \xi_n^2 (t - t')\right] \cos(\xi_n x).$$

$G_i(x, t)$ is the term related to the heat source;

$$G_i(x, t) = \int_{-\infty}^{t} G_i\left(x, t'\right) \mathrm{d}t', \tag{6}$$

where

$$G_i(x, t') = \hat{g}_{0i}(0, t') + 2 \sum_{n=1}^{\infty} \hat{g}_{ni}\left(\xi_n, t'\right) \exp\left[-\alpha_i \xi_n^2 (t - t')\right] \cos\left(\xi_n x\right) \tag{7}$$

and $\hat{g}\left(\xi, t\right) = \int_o^{l_i} g\left(x, t\right) \cos(\xi x)\, \mathrm{d}x$ is the Fourier transform of the heat source function $g\left(x, t\right)$.

Formula (5) is a special case of solution (2-37) presented in [8], for above-assumed boundary conditions. Similar solutions are also valid for the other regions of the cell; function (Eq. 4) should be positioned differently on the x-axis.

2.2 Heat Source

Function $g(x, t)$ stands for the volumetric heat source and corresponds to the amount of energy emitted by the source during non-radiative relaxation into the unit volume per unit time. Assuming that the light pulse comes from the positive side of the x-axis to the element of thickness l_i and absorption coefficient β_i, and is absorbed as described by the Lambert–Beer law, the density function of the volume heat source takes the form of

$$g_i(x, t) = I(t)\beta_i \exp\left[\beta_i \left(x - l_i\right)\right] = I_0 f(t)\beta_i \exp\left[\beta \left(x - l_i\right)\right]. \tag{8}$$

Function $I(t) = I_0 f(t)$ is the intensity of the incident light converted to heat (i.e., its reflected and transmitted parts are neglected); $f(t)$ describes the time shape of the incident light. So, the term related to the heat source (Eq. 7) will take the following form:

$$G_i(x, t) = I_0 f_{\mathrm{N}} \left\{ \left[1 - \exp(-\beta_i l_i)\right] \int_0^t f(t')\, \mathrm{d}t' + \right.$$
$$\left. + 2\beta_i l_i \sum_{n=1}^{\infty} \frac{(-1)^n - \exp(-\beta_i l_i)}{\beta_i{}^2 l_i^2} \cos(\xi_n x) \int_0^t f(t') \exp\left[-\alpha_i \xi_n^2 (t - t')\right] \mathrm{d}t' \right\}, \tag{9}$$

where f_{N} is the normalization constant such that

$$f_{\mathrm{N}}^{-1} = \int_{-\infty}^{\infty} f(t)\,\mathrm{d}t.$$

The energy of the pulse equals

$$E = \frac{I_0 S}{f_{\mathrm{N}}},$$

where S is the cross-sectional area of the input beam. As may be noticed, the calculation may be performed for an arbitrary time profile of the light excitation, for which the integral value in the above expression is finite.

2.3 Solutions for the Whole System

One seeks particular solutions of the general set of equations (Eq. 5), for each of the cell areas, using the second-order boundary conditions (Eq. 2). It results in a set of five integral equations, whose solutions express heat fluxes on the interfaces at any instant of time. To solve that set, a few simplifications have been applied. The time interval $(0, t)$ has been divided into parts 0 to t_1 and t_1 to t, i.e., a time step of $\Delta t = t - t_1$ has been introduced where $t_1 \to t$ (see Fig. 2). Then each of the integrals has the general form,

$$\int_0^t q(t')r(t-t')\,\mathrm{d}t' = \int_0^{t_1} q(t')r(t-t')\,\mathrm{d}t' + \int_{t_1}^{t} q(t')r\left(t-t'\right)\,\mathrm{d}t'.$$

For the first integral for 0 to t_1, the linear approximation can be used, and then the set of integral equations is converted into a set of five algebraic equations for fluxes on interfaces, which is solved numerically step by step for each time instant t, starting

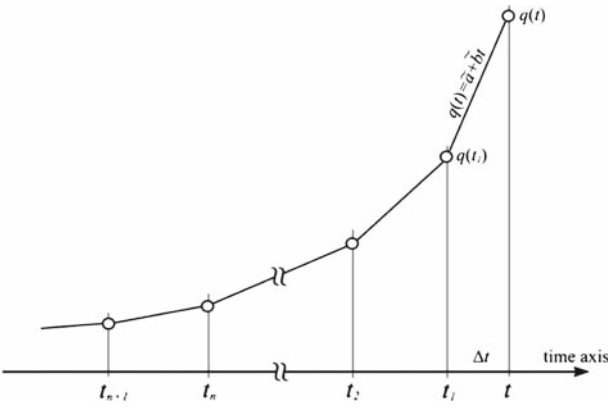

Fig. 2 Linear approximation of the flux $q(t)$ in segment Δt

with $t_1 = 0$, receiving flux values at the material interfaces of the cell in consecutive time moments. These values are used in each step to numerically calculate the values of the expression $T_i(x, t_1)$ at interfaces 0, l, and g using general formulas (Eq. 5) for the respective x, α, and κ.

2.4 Gas Pressure in the Cell

An increase in the cell temperature results in a change of gas pressure. The additional value of the gas pressure in the cell is proportional to the average gas temperature, independent of the thermodynamic process (assumed to be isobaric-adiabatic [1] or isochoric). The coefficient of proportionality changes, depending on the assumed model. For the case of an isochoric process, the gas overpressure equals

$$p(t) = \frac{p_0}{T_0\left(l_\mathrm{g} - l\right)} \int_l^{l_\mathrm{g}} T_\mathrm{g}(x, t)\,\mathrm{d}x. \tag{10}$$

3 Results and Analysis

3.1 General Assumptions

3.1.1 Material and Geometry of the Cell

The cell consists of four areas: backing, sample, gas, and window. It has been assumed that the cell is filled with air at atmospheric pressure. The window and the backing are made of glass that weakly absorbs light. The dimensions of cell elements are listed in Table 1. The thermal and optical properties of respective materials are listed in Table 2.

Table 1 Dimensions assumed for cell elements

Element	Backing	Sample	Gas	Window
Thickness (mm)	2	2	5	2

Table 2 Thermal and optical properties assumed for materials

Material	κ ($\mathrm{W \cdot m^{-1} \cdot K^{-1}}$)	α ($\mathrm{cm^2 \cdot s^{-1}}$)	β ($\mathrm{m^{-1}}$)
Copper	401	1.16	10^8
Graphite	8.10×10^{-2}	6.77×10^{-4}	10^8
Aluminum	237	0.973	10^8
Glass	1.1	6.29×10^{-3}	1
Air	2.60×10^{-2}	0.218	0

3.1.2 Pulse Time Duration and Shape

It has been assumed in the calculations that the light pulse lasts $\tau = 1\,\mu$s and has an energy of 1 mJ. A few time shapes of laser pulses have been applied (Fig. 3):

(a) normal

$$f(t) = t^3 \exp(-at), \tag{11}$$

If the pulse duration τ is understood as the period of time t until the light intensity drops below 5 % of the maximum value, then $a = 10/\tau$;

(b) rectangular

$$f(t) = \begin{cases} 1 & \text{if} \quad t_0 \le t \le \tau, \\ 0 & \text{if} \quad t > \tau, \end{cases} \tag{12}$$

(c) harmonic

$$f(t) = t^3 \exp(-at) \sin^2(\omega t). \tag{13}$$

3.2 Fluxes and Temperature on Interfaces

In order to visualize the heat-flow process in the cell and its influence on gas-pressure changes, calculations have been performed for non-transparent samples of low (graphite) and high (copper) thermal conductivities (for dimensions and thermal properties, see Tables 1, 2). Light absorption has been assumed to exist in the sample and in the glass of the cell window. External surfaces of the window and of the backing are maintained at the temperature of the surroundings T_0.

Figure 4 shows the time evolution of heat fluxes through material interfaces of the cell and their temperature values as a function of time. Since the positive direction of the heat flux is the same as the positive direction of the x-axis (Fig. 1), heat flow fluxes directed in the negative direction of this axis are shown in the charts as negative.

The curves for interfaces $x = \mathrm{w}, \mathrm{g}, \mathrm{l}, 0, -\mathrm{b}$ (see Fig. 1) are consecutively shown. The interpretation of the presented results is as follows:

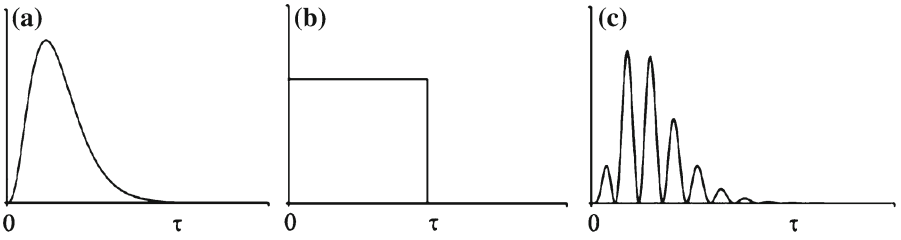

Fig. 3 Time shapes of laser pulses

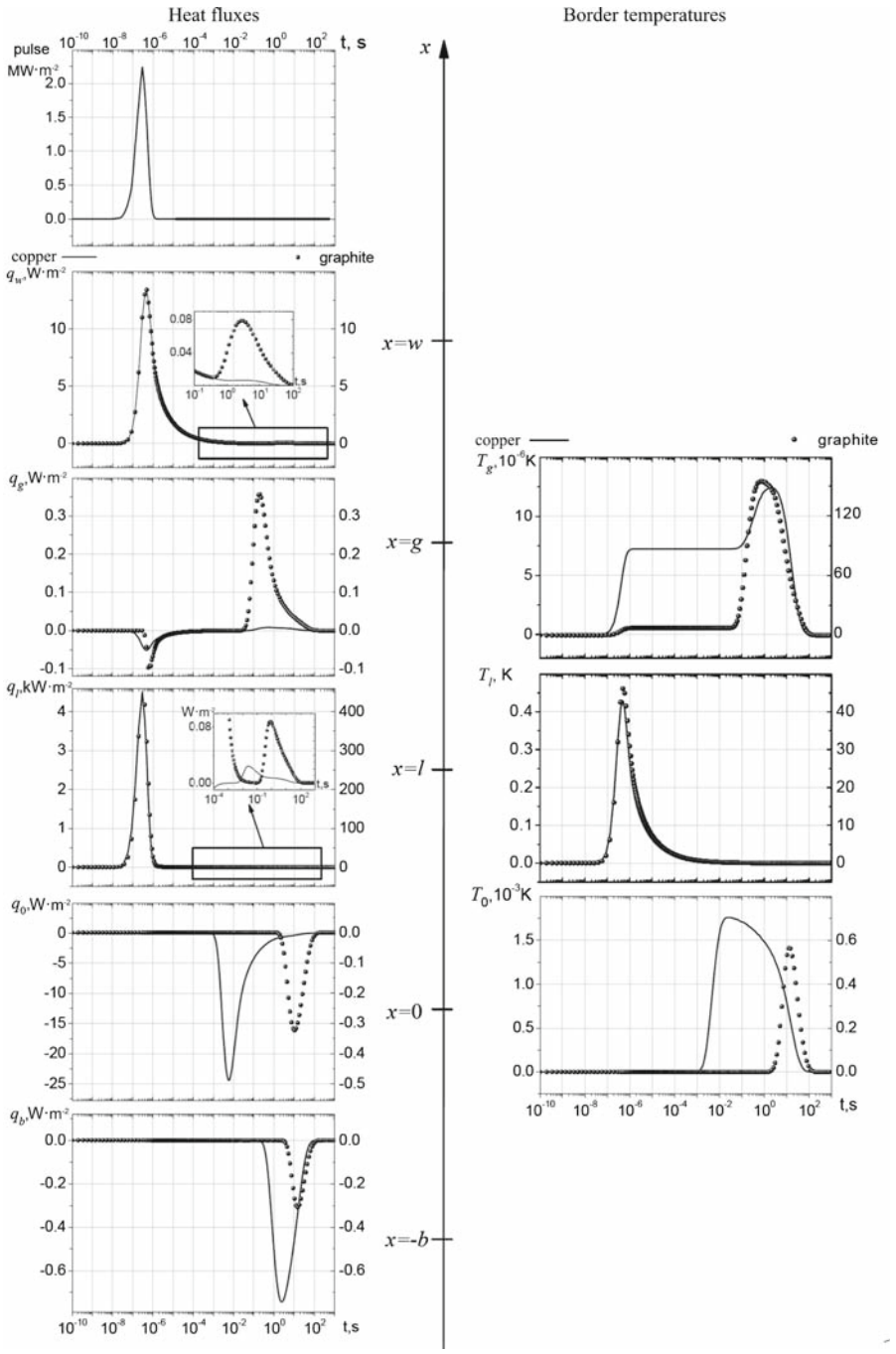

Fig. 4 Interfaces: time evolution of heat fluxes and border temperature rises

$x = \mathrm{w}$: The external surface of the window and, at the same time, external surface of the cell are maintained at room temperature. Electromagnetic radiation is absorbed in the entire depth of the window. The heat flux is directed here from the window into the surroundings (for $x > \mathrm{w}$), having, therefore, a positive sign. For both samples flux curves are identical in the initial time instants. The small chart presents the area where the fluxes cease to be identical. The temperature of this surface is constant, which results from the assumptions of the model.

$x = \mathrm{g}$: Interface window–gas. This is where the heat exchange between the window and the gas inside the cell occurs. The heat flux is several orders of magnitude lower, compared to that on the interface w, since the gas filling the chamber weakly carries heat away from the window. During the pulse duration, the heat flux has a negative sign because the heat flows from the heated window to the non-heated gas, in the negative direction of the x-axis. For the case of both samples, the values of the heat fluxes are identical after approx. 0.1 s, related to the moment when the heat disturbance from the sample surface reaches the considered interface. The maximum value is higher for weakly heat-conducting graphite. The presence of the heat source in the window results in an increase of temperature on the interface g immediately after switching on the pulse. At later time moments, one can see stabilization and a significant increase of the temperature after a heat disturbance originating on the sample surface reaches the interface.

$x = \mathrm{l}$: The front side of the sample is illuminated by the light pulse. The strongest light source in the entire system is found close to the surface of the sample (for the assumed value of the optical absorption coefficient for both samples, the optical absorption depth equals 10^{-8} m). The surface of the sample heats the gas inside the cell–the heat flux is positive. A good conducting sample (copper) quickly transfers heat from near the surface to its depth; the temperature gradient is many orders of magnitude lower than in the case of graphite (right vertical axis). Heat fluxes differ by two orders of magnitude and have similar time profiles. The temperature of the front side of the sample increases with the appearance of the light pulse and decreases after it ends. The interface temperature values are higher for the graphite sample. The small chart presents these fluxes on an enlarged scale. For both materials an increase of flux values is observed in this area. This increase results from the arrival of a thermal wave, propagated through the sample and reflected from the sample–backing interface to the sample surface.

$x = 0$: Rear side of the sample. When the disturbance reaches the backing after propagating through the entire thickness of the sample, the heat flux through this surface increases. It is directed from the sample toward the backing, so it has a negative sign. Due to the high thermal conductivity of a copper sample, its flux increases much earlier than that of a graphite sample, and its values are higher. The temperature of the backing surface on the side of the sample increases with an increase of the heat flux and decreases at later times. The final decrease is observed when the heat reaches the external surface of the cell, maintained at the temperature of the surroundings, and is conducted outside.

$x = -b$: Rear side of the backing, maintained at the temperature of the surroundings. The flux observed in the case of copper appears much earlier than for graphite. Heat flux values for both samples have comparable values. The temperature increase on this surface equals zero, which results from assumptions of the model.

3.3 Temperature Field Inside the Cell

Figure 5 presents the spatial temperature profile inside the cell containing the copper sample for early times; an exact time moment for which the profile has been calculated is specified in the right-upper corner of each chart. The highest temperature is observed on the surface of the sample. At the following time moments, the heat is

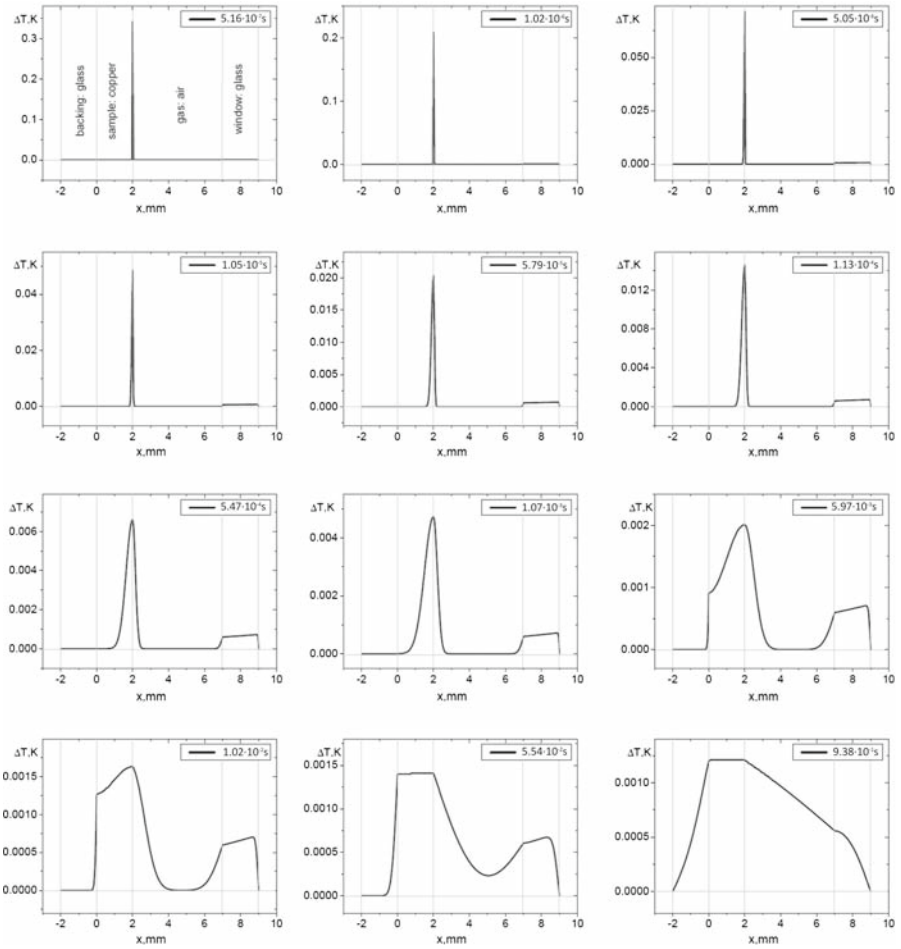

Fig. 5 Temperature field evolution in the cell with copper sample

distributed toward the sample and the gas. The temperature of the window increases already during the duration of the pulse, but the increase being several orders of magnitude lower than the sample's surface temperature, is not visible on the charts until the sample cools to temperature values comparable with those of the window. The high thermal conductivity of copper causes significant amounts of heat to be generated in the region close to the surface, resulting in a flow from the sample–gas interface toward the sample and the backing.

The temperature field for consecutive time moments, for a cell with a graphite sample, is presented in Fig. 6. The warmest area of the cell is located on the sample surface. The heat does not propagate into the depth of the sample as quickly as in the case of copper, and the temperature gradient in the carbon sample is larger. It is also visible in the difference of the heat flux values through the surface of the sample—see

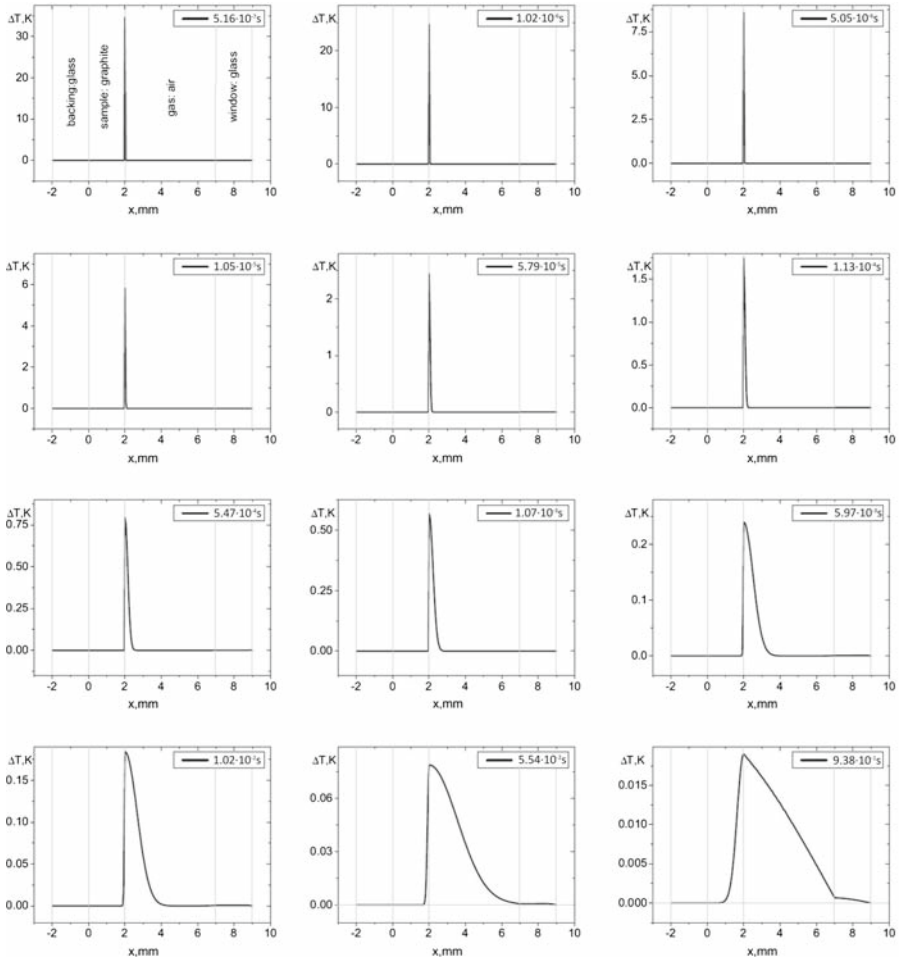

Fig. 6 Temperature field evolution in the cell with graphite sample

Fig. 4c. Maximum temperature values on the light absorbing surface of the sample are also many times higher than for the case of copper.

For the case of copper, the sample heat wave propagates into the depth of the sample very quickly, due to its high thermal diffusivity (this parameter determines the velocity of isothermal surface propagation inside the material [6]), which is four orders of magnitude lower for graphite in comparison with copper. At early times, when the temperature inside the copper sample has already stabilized, it has only increased on the surface and within a small distance into the depth of the carbon sample. The copper sample starts to emit heat from its rear surface to the backing much earlier than for the carbon sample. The external surface of the backing is kept at the temperature of the surroundings, and for the case of the cell with a copper sample, the heat flow through this interface begins earlier than for the case of the graphite sample. Temperature values for the graphite sample are much higher. This results from its heat capacity value, almost three times higher than for graphite. Light absorption in the window also heats the gas from the window side. The heat disturbance propagates inside the gas from both the window and the sample side.

The following conclusions are drawn from a field temperature analysis. The maximum temperature of the front surface of the sample strongly depends on the thermal properties of the material. For the case of high thermal-conductivity samples, one observes a slower decrease of the surface temperature for longer pulses, resulting from reflection of the heat disturbance from the sample–backing interface (this effect is observed for weakly conducting materials of the backing under the sample). Such an effect is stronger for thin samples. The temperature of the rear surface of the sample depends strongly on its thickness and thermal conductivity coefficient value. As is the case for pressure, the technical possibility to measure the temperature of the front side of a transparent sample is limited by a low signal level. The use of a backing material with a high light absorption coefficient value allows an increase of the level of the received signal. Registration of the front surface temperature then yields similar information to that resulting from temperature measurements in the pulse-flash method [2].

3.4 Gas Pressure

Time profiles of the gas pressure in the cell of dimensions from Table 1, with copper and graphite samples, are shown in Fig. 7b (Fig. 7a demonstrates the light pulse shape). The curves are shown on a logarithmic scale, since it reveals both fast and slow changes of the observed parameter.

Gas is heated mainly through the sample surface. The obtained values of the gas pressure are higher for the sample with a higher surface temperature. In the curve obtained for the copper sample, one may see three sections: an increase, longer-time stabilization with a high peak at the end, and then final decay. For the case of the graphite sample, the curve is more regular, consisting of the growth area over the time of the pulse duration, a stabilization area with a small local peak, before a final decrease. Hence, without any doubt, the pressure inside the cell is a function of the sample's

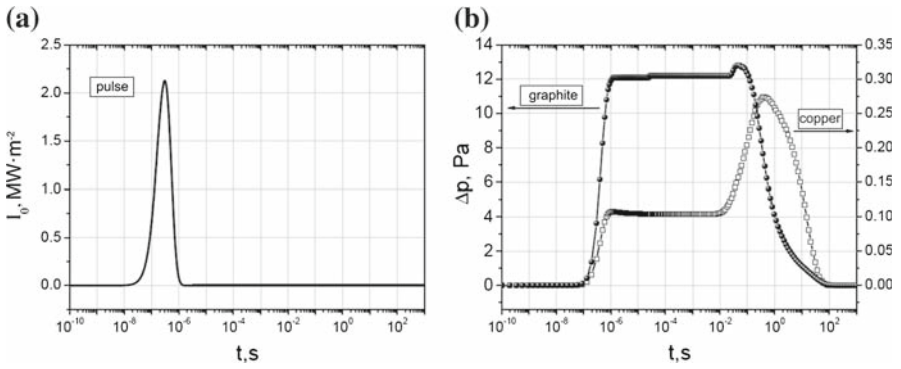

Fig. 7 (**a**) Light pulse time shape and (**b**) time profile of gas pressure in the cell containing copper sample (*rectangles*, right axis) or graphite sample (*circles*, left axis)

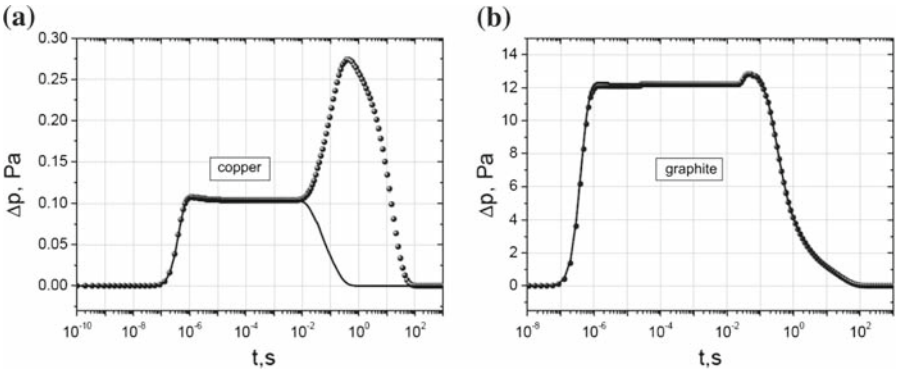

Fig. 8 (**a**) Gas pressure in the cell with 2-mm copper sample without backing (*solid line*), with 2-mm glass backing (*circles*); (**b**) graphite sample (*overlapped curves*)

thermal properties. This implies usefulness of pulse photoacoustic investigations in measurements of thermal properties of solids.

A very large second increase of the pressure for the copper sample is related to its high thermal conductivity. This increase is caused by the thermal pulse reflected from the sample–backing interface that traveled back through the sample and reached the gas, resulting in a significant increase of its temperature and pressure. It is visible in Fig. 8a, which shows changes of the gas pressure in the cell with a 2 mm thick copper sample without backing (solid line). The rear surface of the sample maintains the temperature of the external surrounding medium. Black circles show the pressure curve in the cell with glass backing. In this case, the second pressure increase is present so it has to be related to the reflection of the thermal disturbance propagating in the sample from the sample–backing interface. Similar calculations have been performed for graphite, Fig. 8b. Graphite has a low thermal conductivity and the thermal pulse decays nearly completely while traveling through the sample.

Gas overpressure in the photoacoustic cell is proportional to the average temperature of the gas filling the cell, and its temperature is inversely proportional to the gas

height (Eq. 10). So, with an increase of the cell length, one observes lower values of the gas pressure. Pressure curves for a graphite sample are shown in Fig. 8b on a logarithmic time scale. The curves differ in height. The biggest pressure increase is observed in the shortest cell, since it contains the least amount of gas to be heated. As the gas length increases, the decrease of pressure is delayed.

Figure 9b presents pressure curves normalized to one on a linear time scale. With an increase of the cell length, the curves are less inclined to the time axis—and return of pressure values to the state of equilibrium is delayed.

The dependence of the maximum gas pressure on the gas length is shown in Fig. 10a. It decreases with an increase of the cell length and is directly proportional to the inverse gas length, as shown in Fig. 10b.

The shape of the gas-pressure curve in the cell depends on the pulse duration time. To illustrate that, calculations for a rectangular pulse—the simplest of all pulse shapes—have been carried out. For that purpose, pressure curves in the cell with a high-conducting copper sample and weakly conducting graphite have been carried out for different pulse duration times from 10^{-8} s to 10^{-1} s. The pulses have been normalized in different ways: to the pulse energy of 1 mJ and to the light intensity $I_0 = 1.5 \times 10^7\,\mathrm{W \cdot m^{-2}}$.

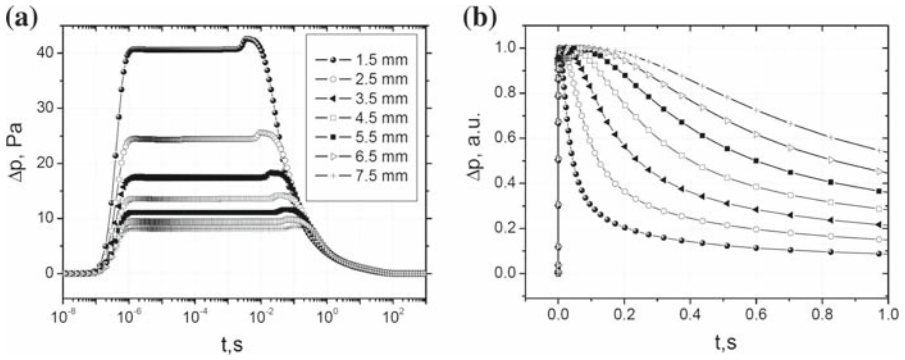

Fig. 9 Gas pressure in the cell with different gas lengths for a graphite sample

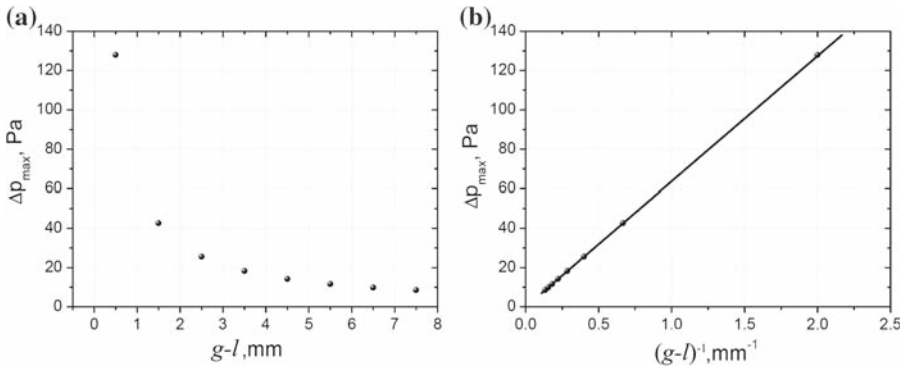

Fig. 10 Dependence of maximum gas pressure on the gas length for a graphite sample

Figure 11 presents calculation results for a cell with (a) copper and (b) graphite samples for pulses normalized to the pulse energy. The curves differ from one another only in the pressure increase phase, i.e., during pulse duration. When the entire energy is delivered to the system (same for all cases) and the pulse has been finished, then for the given pulse the gas pressure reaches a slightly higher value than for the case of short pulses, but it normalizes at the following times and becomes identical as for the case of curves for shorter pulses. Since all pulses carry the same amount of energy, the shortest pulse has the highest light intensity, which causes a significant temperature growth of the sample surface and makes the initial pressure in the cell higher than for the case of longer pulses.

One should notice that for all pulses the maximum value of the gas pressure occurs at the same time and its decrease follows the same curve. For the case of rectangular pulses of the same light intensity I_0 but different duration times (Fig. 12), the initial part of the pressure increase process is identical for all curves, since the system absorbs a light beam of intensity I_0. The longer the sample is illuminated, the higher is the

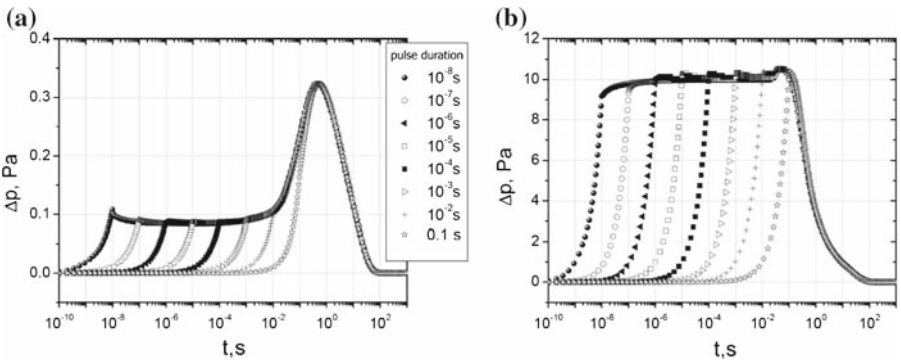

Fig. 11 Pressure shapes for different pulse durations, normalized to the pulse energy for (**a**) copper and (**b**) graphite samples

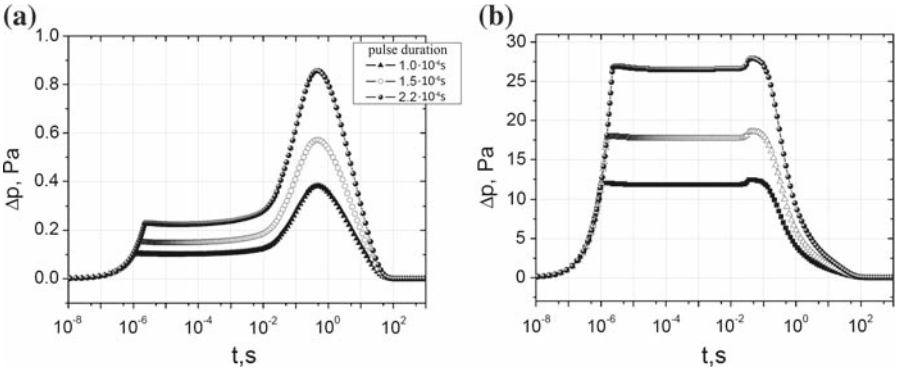

Fig. 12 Pressure shapes for different pulse durations, normalized to the light intensity for (**a**) copper and (**b**) graphite samples

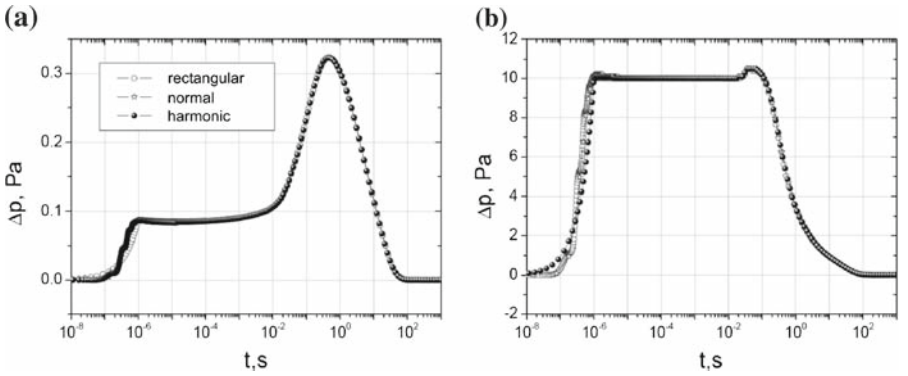

Fig. 13 Influence of pulse shape on gas pressure: (**a**) copper and (**b**) graphite

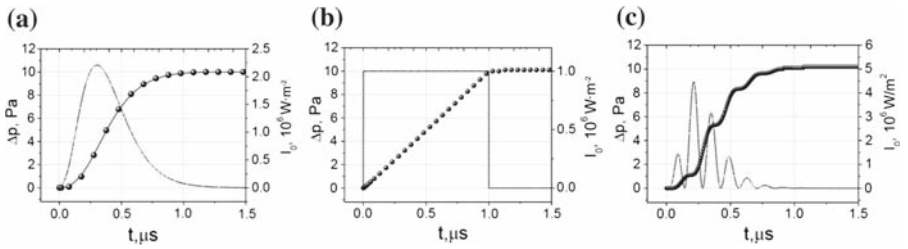

Fig. 14 Influence of pulse shape on gas pressure: graphite sample, pulse of energy 1 mJ; (**a**) *normal*, (**b**) *rectangular*, and (**c**) *harmonic*

pressure in the cell. Curve shapes for all pulse duration times are similar; they differ only in peak values.

The influence of the pulse shape with time on the pressure curve in the cell of dimensions backing/sample/gas/window (2/2/5/2) mm, has been analyzed for three different pulse types: normal (Eq. 11), rectangular (Eq. 12), and a series of pulses, called the harmonic pulse (Eq. 13). It has been assumed that their duration times and energies are identical—1 s and 1 mJ, respectively. Results are presented in Fig. 13 for (a) a copper sample and (b) a graphite sample. The curves differ only in the pressure growth phase, during the pulse-duration period. The same energy is delivered to the system, so the curves become identical when the pulse has ended. The initial parts of the shapes on a linear time scale are presented in Fig. 14.

3.5 Verify the Correctness of the Model

To verify the correctness of the proposed model, comparisons with existing theory of the pulse photoacoustic effect in solids—the theory of Parker et al. [2]—have been performed. Figure 15 presents a comparison of temperatures of the rear side of the sample resulting from both theories for copper and graphite as a function of time. Points marked with circles result from Parker's theory, while solid lines are results of calculations made with the new model. The vertical axis shows temperature changes

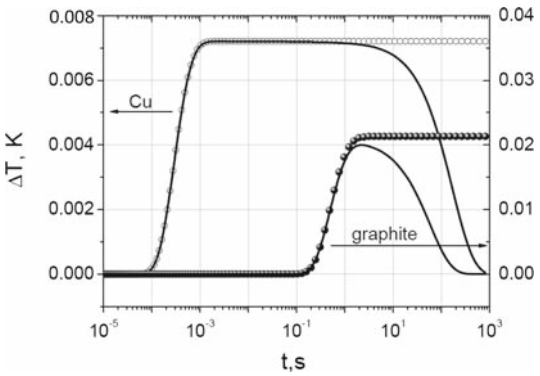

Fig. 15 Comparison with Parker's model: temperature of the rear side of the plate for copper and graphite samples of 0.5 mm thickness

measured in absolute units. Resulting curves are identical to those for the initial times. The theory of Parker assumes that, as has been mentioned earlier, the plate is thermally isolated, which leads to stabilization of its temperature after a certain time. The new model assumes heat transfer from the sample to the surroundings which returns the system to its initial state and lowers its temperature, including the rear surface of the sample.

Critical to the theory of Parker et al., the stage of temperature rise on the rear side of the sample is the same as in the new model; therefore, it should yield correct values of the sample's thermal-diffusivity coefficients, determined using $\alpha = 1.38l^2/\pi^2 t_{1/2}$. One may expect to see differences between both theories for the case when the sample's surroundings conducts a heat well. Results of calculations performed for a copper plate on a 5-mm aluminum backing are shown in Fig. 16. Temperature values of the rear surface of the plate, resulting from both models, differ significantly, but as is visible on the graph where the temperature values calculated with the new theory are normalized to the maximum temperature value of Parker's theory, $t_{1/2}$ for time instants are the same for both cases.

The thermal-diffusivity values resulting from Parker's formula, applied to times $t_{1/2}$ determined for other materials using the proposed model, are presented in Table 3. The magnitude of the error of the determined values decreases with an increase of the thermal diffusivity. For the case of graphite, the error value has the highest value and reaches 4.4 %. The thermal diffusivity of graphite is very low, and the time until the rear surface of the sample reaches half of its maximum value equals about 0.5 s, which is very long compared to the pulse duration time of 1 μs. In the article of Parker, the cited method of measurement has been applied for good thermally conducting samples, such as copper, iron, nickel, aluminum, tin, and a few alloys.

The next theory that the results received from the new model may be compared to is the theory of Mandelis and Royce (MR theory) [4]. The temperature and the pressure of the gas have been calculated on the basis of Eqs. 15 and 17 from the cited work, for optically and thermally thin and thick samples (after appropriate modifications). The thermally and optically thick sample has been assumed to have thermal parameters of rubber (data used for calculations in Table 2). In addition, the half-infinite window, a backing material with thermal properties of glass, and air as a gas have also been assumed. The gas height value has been set to 3 mm. Light absorption has been

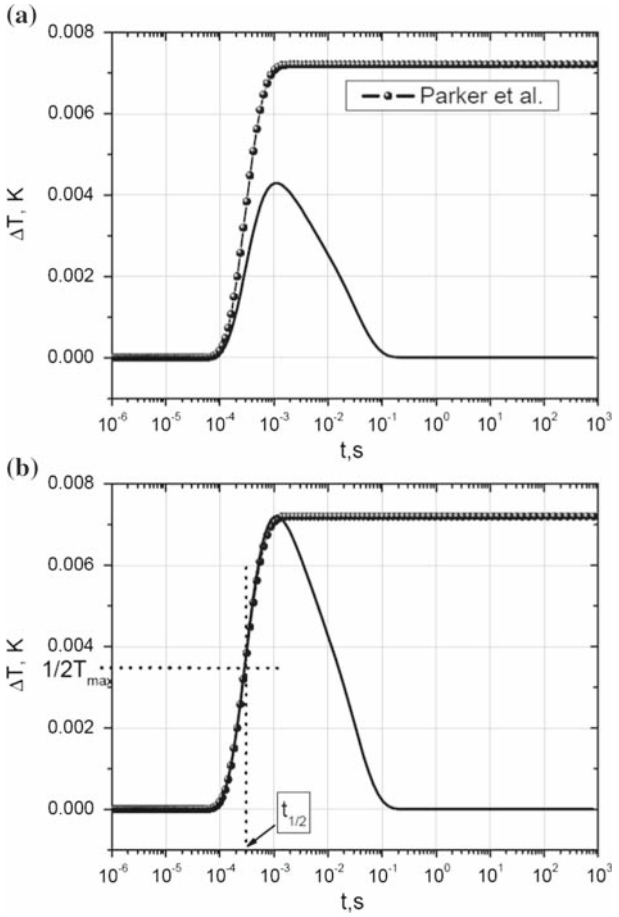

Fig. 16 Comparison with Parker's Model. (**a**) Temperature of rear side of the sample with well-conducting backing (sample, 0.5 mm copper; backing, 5 mm aluminum). (**b**) Temperature field resulting from the new model has been normalized to the maximum temperature value from Parker's theory

Table 3 Values of the thermal diffusivity α, resulting from presented model of the cell

sample	α ($m^2 \cdot s^{-1}$)	Calculated α ($m^2 \cdot s^{-1}$)	Error (%)
Cu	1.16×10^{-4}	1.16044×10^{-4}	0.04
Al	9.73×10^{-5}	9.73653×10^{-5}	0.07
Pb	2.40×10^{-5}	2.39907×10^{-5}	0.04
P	1.68×10^{-7}	1.70921×10^{-7}	1.71
Graphite	6.77×10^{-8}	7.06804×10^{-8}	4.40

assumed to exist only in the sample; absorption in the window has been neglected. A sufficiently large window and backing lengths have been taken into consideration, since these elements are half infinite for the case of the MR theory.

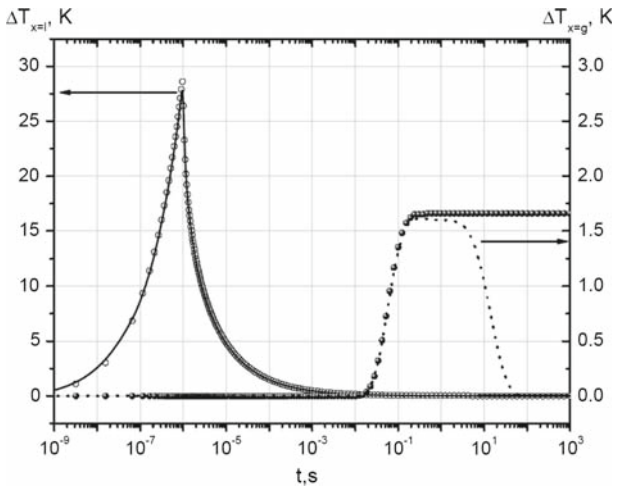

Fig. 17 Comparison with MR theory: thermally and optically thick sample (rubber 1 mm)—temperature on interfaces sample–gas ($x = \mathrm{l}$) and gas–window ($x = \mathrm{g}$)

The MR theory authors have restricted cell dimensions to very small values (gas—0.1 mm, sample—10 μm). This has been done to limit the number of terms in the series expressing the temperature and pressure values to 25 to 30, and has been most likely caused by the limited computational power available at that time (1979 and 1980). For a cell with an optically and thermally thick sample, the temperatures of the front surface of the sample ($x = \mathrm{l}$) and the window surface ($x = \mathrm{g}$) have been calculated as functions of time.

The results of these calculations are shown in Fig. 17. For a temperature on the interface ($x = l$), one finds very good consistency between both the models. For the window–gas interface, the MR theory results are up to a certain moment in agreement with those of the new model. Since the window for the MR theory is half infinite and its thermal diffusivity is weak (glass), heat transfer into the depth of the window is very slow, and in the time period shown in Fig. 17, the surface temperature does not decrease. The phase of the growth and maximum values of the window's surface temperatures are in agreement.

4 Comments on Results of Analysis

After illumination with the light pulse, the heat transfer process from the sources created as the result of light absorption to other elements, begins in the cell. The thermal disturbance is reflected from material interfaces inside the cell. The final temperature distribution in the cell is determined by the thermal properties of its elements. The gas in the cell is heated differently when the sample is characterized by a high thermal conductivity and again differently if it weakly conducts heat. The gas pressure is therefore dependent on the sample type, and its time shape carries information on the sample. The analyses demonstrate that the initial part of the pressure curve depends

strongly on the sample type. The remaining portion of the curve is dependent on other cell elements, especially on the gas height.

The following conclusions have been drawn from simulations of the pressure curves:

1. Pressure profiles for non-transparent and transparent samples depend on the sample's thermal-conductivity coefficient. This gives the possibility to work out the method of determining thermal parameters of the sample from measurements of the time–pressure profile.
2. The pressure profile depends on the sample thickness.
3. The pressure amplitude of the gas inside the cell depends on the sample's thermal-conductivity coefficient. For the case of non-transparent samples, the higher is the thermal conductivity, the lower is the maximum overpressure value achieved. For the case of transparent samples, the signal amplitude increases with an increase of the sample's thermal-conductivity value.
4. If possible, samples for measurements should have a smaller thickness for the case of a weakly conducting material and a larger thickness for the case of a good conducting material. If such material preparation is not possible, one may observe an initial signal part for good conducting samples and a later signal part for weakly conducting samples.
5. Investigations of materials with a low light absorption coefficient value are limited by a very low signal level. In such cases one may apply a backing material with a light absorption coefficient value under the sample. The gas pressure depends in such cases on the amount of heat and the time it needs to travel from the backing surface to the window, i.e., it depends on the thermal parameters of the sample under investigation.

Summarizing, the pressure wave shape in the cell depends strongly on the sample and cell dimensions. The bigger are these elements of the cell, the lower are the increases of gas pressure and the photoacoustic signal. One should attempt to minimize longitudinal dimensions of the cell. Its transverse dimensions need to be chosen appropriately to allow a description of the experiment with a one-dimensional theory. In a cell with static element dimensions, exchange of the sample for another one with a different thickness automatically changes the gas-length value. It is useful when the gas-length value may be adjusted to allow carrying out measurements with a fixed value for all investigated samples.

5 Conclusions

This article presents a one-dimensional photoacoustic cell model, consisting of four, finite-length elements: backing, sample, gas, and window. The model is based on the solution of a system of parabolic heat equations for a layered structure, assuming ideal heat flow between its elements. It allows use of initial pulses of arbitrary time shape and duration and takes into account light absorption in any area of the cell. This feature makes it universal.

The complicated form of general solutions of the heat equation system resulted in application of numerical methods. The obtained results have been compared to

those of two other known theories, confirming a high level of agreement among these results, which demonstrates the correctness of the model. At the same time, it should be emphasized that the developed theory is more universal than the existing ones. A new element here is the possibility to use any time shape of the incident pulse and introduce absorption of light in any of the cell's elements. The presented system has a backing and window of finite length, while known theories assume infinite dimensions for these parts.

References

1. A. Rosencwaig, A. Gersho, J. Appl. Phys. **47**, 1 (1976)
2. W.J. Parker, R.J. Jenkins, C.P. Butler, L.G. Abott, J. Appl. Phys. **32**, 1679 (1961)
3. L.C. Aamodt, J.C. Murphy, J. Appl. Phys. **49**, 3036 (1978)
4. A. Mandelis, B.S.H. Royce, J. Appl. Phys. **50**, 6 (1979)
5. A. Mandelis, B.S.H. Royce, J. Appl. Phys. **51**, 1 (1980)
6. A.V. Luikov, *Analytical Heat Diffusion Theory* (Academic Press, New York, 1968)
7. M. Necati Ozisik, *Boundary Value Problems of Heat Conduction* (Dover Pubs. Inc, Mineola, NY, 1989)
8. H.S. Carslaw, J.C. Jaeger, *Conduction of Heat in Solids* (Clarendon Press, Oxford, 1989)